Determination of safe speeds for a coach travelling on a floating bridge

Transportation Research Interdisciplinary Perspectives 34 (2025) 101736

Contents lists available at ScienceDirect

Transportation Research Interdisciplinary Perspectives

journal homepage: www.sciencedirect.com/journal/transportation-research-interdisciplinary-perspectives

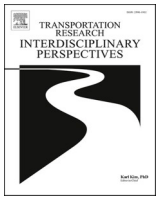

Determination of safe speeds for a coach travelling on a floating bridge

Dragan Sekulic [a,*], Alexey Vdovin [a], Bengt Jacobson [a], Simone Sebben [a], Stian Moe Johannesen [b]

[a] Chalmers University of Technology, Gothenburg, Sweden
[b] The Norwegian Public Road Administration, Oslo, Norway

ARTICLE INFO

Keywords:
Safe speeds
Floating bridge
Storm conditions
Wind loads
Lateral stability
Tracking ability

ABSTRACT

Coastal highway route E39 is immense road project in Norway with the aim to shorten the journey time between the south part (Kristiansand city) and the north part of the country (Trondheim city). Different high-tech structures will make E39 route continuous and reduce the travel time from currently 21 h to 11 h. A floating bridge has been considered for Bjørnafjorden. This paper suggests bus safe speeds for travel on a floating bridge exposed to 10 different storm conditions (W1–W10). The results show that the coach does not stray from the traffic lane under mild storm conditions (W1–W2) even for the highest vehicle speed of 108 km/h. However, at a speed of 90 km/h for W6 and W7 and at a speed of 72 km/h for W8, the vehicle severely and often departures the traffic lane. At 36 km/h, 54 km/h and 72 km/h for strong storms (W9–W10), the windward rear wheel of the bus frequently loses contact with the floating bridge deck.

Introduction

The E39 route, in Norway, is 1100 km in length connecting the south part (Kristiansand city) with the north part of the country (Trondheim city). There are several fjords crossed by ferries on this route which makes the journey time long, over 20 h. Coastal highway route E39 is immense road project in Norway with the aim to shorten the journey time. In the reconstruction of E39 route, ferries will be replaced with the high-tech structures (e.g. floating and suspension bridges, submerged floating and subsea road tunnels) making the route continuous and journey time considerably lower, around 11 h (Vegvesen, 2017). Improved E39 route will bring various benefits for both freight and passenger transport (e.g. lower driving and time costs (Vegvesen, 2021)).

Dependable transportation on the reconstructed E39 route seeks for safety measures suited for hazardous conditions during driving. This is crucial for structures like long-span bridges exposed to strong winds and waves during bad weather. Wind-vehicle-bridge interactions for long-span bridges have been investigated in previous studies (Han et al.; Wang et al., 2014). The entire safety performance of vehicles in realistic stochastic traffic moving through highway infrastructure systems was assessed using an integrated approach in (Hou et al., 2019). For demonstration reasons, the suggested approach was used on a bridge-roadway system. According to one of the study's findings, trucks had a little higher accident rate on dry roads than vans and cars (Hou et al., 2019).

For Bjørnafjorden, floating bridges have been proposed as a possible crossing option (Fig. 1b). The effects of the vertical motion of floating bridges on the ride comfort of bus drivers were analysed at different vehicle speeds based on numerical simulations (Sekulic et al., 2020; Sekulic, 2018) and a driving simulator (Gustafsson et al. 2019). The effects of floating bridge motion and wind excitation on the tracking and lateral stability of buses and driver loads under 1-year storm conditions were recently investigated (Sekulic et al., 2021; Bhat et al. 2020). At a speed of 108 km/h, a rollover risk was confirmed for a bus since the windward wheels lost contact with the floating bridge deck (Sekulic et al., 2021). The simulation findings indicate that a bus might start journey on floating bridge at a lower speed (e.g., 72 km/h) under wind loads from 1-year storm condition, with the option to increase speed (up to 90 km/h) after about 2 km (Sekulic et al., 2021).

Bjørnafjorden is located to the south of Bergen and is exposed to wind and waves from the North Sea (Fig. 1a). It is important to know how a bus would behave under various storm conditions, i.e., for conditions more and less severe than those for a 1-year storm (Table 1). This paper investigates the lateral stability of a coach travelling on a floating bridge exposed to 10 different storm conditions (W1-W10). The main aim of

* Corresponding author.
E-mail addresses: dragan.sekulic@chalmers.se (D. Sekulic), alexey.vdovin@chalmers.se (A. Vdovin), bengt.jacobson@chalmers.se (B. Jacobson), simone.sebben@chalmers.se (S. Sebben), stian.moe.johannesen@vegvesen.no (S.M. Johannesen).

https://doi.org/10.1016/j.trip.2025.101736
Received 26 November 2022; Received in revised form 4 November 2024; Accepted 9 November 2025
Available online 18 November 2025

this work is to determine the safe travel speeds for buses under 10 different storm conditions. In the past, safety measures for bridges under the influence of the strong wind were commonly established regarding subjective experience (Chen and Cai, 2004), without consideration of the results from numerical investigations. This work has potential practical application to recommend safe speeds and assist floating bridge management in severe weather conditions.

Coach model

In this work, a two-rigid-axle coach with eight degrees of freedom (DoFs) is employed for the numerical investigation. Detailed description of the mathematical model could be found in (Sekulic et al., 2021). Vehicle lateral and yaw motion *(y, ψ)* are considered for the in-ground-plane DoFs (Fig. 2a). The out-of-ground-plane DoFs include bouncing of the sprung mass, front and rear axles, the sprung mass roll motion, and the front and rear axles roll motion *(z, z_1, z_2, φ_{xs}, φ_{x1}* and *φ_{x2})* (Fig. 2b). Coach parameters from Fig. 2 and their values used in the simulations are given in Appendix section (Table A4).

The active and inertial forces and moments for in-ground-plane motions are presented in Fig. 2a. The derivation of differential equations of motion for both in-ground-plane and out-of-ground-plane DoFs and their final forms were provided by (Sekulic et al., 2021). Numerical simulation and coach modelling are both done using MATLAB/Simulink software.

Vehicle model excitation

Hydrodynamic and wind loads for ten different storm conditions (W1-W10) were used as inputs for bridge model excitation. The Orcaflex software was used to simulate the bridge responses to obtain time series data (Vegvesen, 2017). The definitions of the storm conditions are given in Table 1.

Each storm condition is described by waves, swells and wind characteristics (Table 1). Waves are generated locally at the site of the floating bridge by the wind (i.e., from the friction of the sea surface and the wind) and are short periodic waves. Swells are waves that have travelled over the ocean and reach Bjørnafjorden from the North Sea. These waves are long periodic waves generated from storms far from the floating bridge location. The overall wave conditions (both wind-generated waves and swells) at the surface elevation of the bridge are simulated by superimposing waves generated from two Jonswap spectra (Vegvesen, 2017). A Kaimal wind spectrum was used to create a wind field (Branlard, 2010) with mean wind speed *ws* (Table 1) and the turbulence characteristic I_u, as shown in Eq. (1).

$$I_u = \frac{1}{ln\left(\frac{z}{0.01}\right)} \tag{1}$$

where *z* is the height [m].

Waves, swell and wind are characterized with parameters – wave and wind direction (Dir [°]); wave height (Hs [m]); a peak period (Tp [s]); and mean wind speed (ws [m/s]), (Table 1). It could be noticed that height of the wind-generated waves are higher values with shorter peak periods compared to swells waves (Table 1).

The coach model was excited with vertical ($z_{br}(vt)$), lateral ($y_{br}(vt)$) and roll motions ($\varphi_{br}(vt)$) of the floating bridge and wind loads (Fig. 3a). To determine the relative wind velocity ($V_{rel\ wind,\ x,y,z}$), wind velocity signals ($V_{wind,\ X,Y,Z}$) from the global (earth) coordinate system *OXYZ* were converted into the vehicle coordinate system O_1xyz (Fig. 3b). This procedure could be found in (Sekulic et al., 2021). Aerodynamic forces and moments acting on the coach are calculated considering relative wind velocity signals and used when defining differential equations of motion. The equations for aerodynamic load calculations were defined in (Sekulic et al., 2021).

Bridge motions (vertical, lateral, roll motions) under the influence of environmental loads (wind and waves for storm conditions) were obtained by simulation using *Orcaflex* software. Vertical (z_{br}), lateral (y_{br}) and torsional (φ_{br}) displacements of the bridge deck centre (point C, Fig. 4) were given for specific points along the length of the bridge (on each 5 m or on each 8 m depending on the bridge nodes definition in the *Orcaflex* software) as a function of simulation time which is one hour (3600 s). It means that input data for the coach model depend on vehicle position on the bridge deck and time. Consequently, bridge motion data will not be the same for the different vehicle speed.

Vertical bridge excitation

Fig. 5a presents vertical bridge displacement data for a few points (at 0.6 km; 2 km; 5 km) in function of simulation time for a 1-year storm

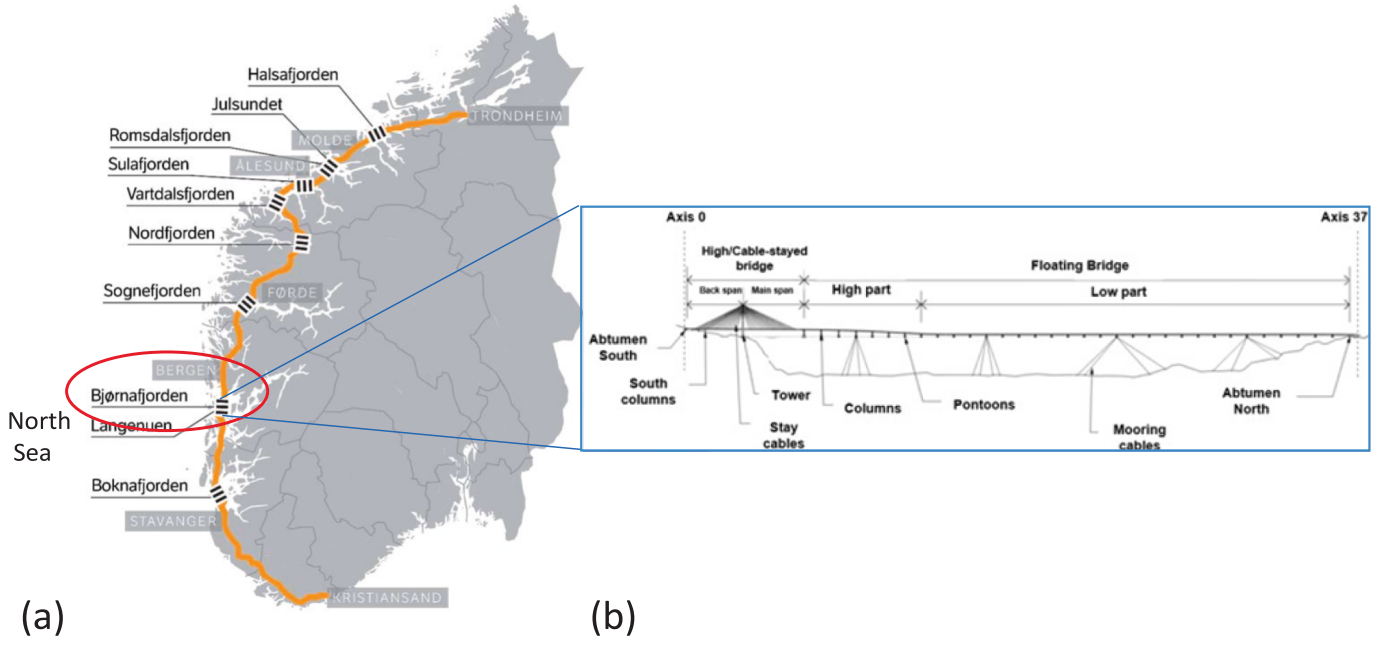

Fig. 1. Bjørnafjorden a) location, and b) floating bridge (straight concept solution).

(W6). It could be seen that vertical bridge displacement on distance at 2 km differs for two chosen vehicle speeds of 36 km/h and 90 km/h Fig. 5b). From bridge motion data set we defined vehicle input data set. Detail procedure could be found in (Sekulic et al., 2021).

Fig. 6 shows the vertical bridge excitation for five different vehicle speeds (36 km/h, 54 km/h, 72 km/h, 90 km/h and 108 km/h) and W1–W10 conditions. These excitation cases encompass vertical bridge motion and road roughness of A/B quality (A/B road class refers to the road of very good/good quality defined by ISO 8608, (1995) standard). More modelling information for road roughness could be found in (Sekulic et al., 2020). The excitation magnitude gradually increases with the storm severity. For a mild storm (W1), vertical bridge excitation is small and within ± 0.05 m (Fig. 4a). For the strongest storm (W10), vertical bridge excitation is large and within ± 0.6 m (Fig. 4j).

Lateral bridge inputs (motion and velocity)

Fig. 7 shows the lateral bridge motion for five different vehicle speeds. The magnitude of lateral motion gradually increases with the storm severity. For W1, lateral motion is small and within ± 0.2 m (Fig. 7a). For the strongest storm, W10, lateral motion excitation is considerable and within ± 1.9 m (Fig. 7j). Lateral bridge motion has been used as an input for vehicle driver model when calculating wheel steering angle. The driver model was defined by the path tracking pure pursuit method. Detail information about driver model could be found in (Sekulic et al., 2021).

The lateral bridge velocity for five different vehicle speeds is shown in Fig. 8. These signals were used for lateral tire forces calculations (Sekulic et al., 2021). For W1, the lateral velocities are small and within ± 0.1 m/s (Fig. 8a). For the strongest storm, W10, the lateral velocity values are high and within ± 0.7 m/s (Fig. 8j).

Bridge roll motion

Fig. 9 shows bridge roll motion for five different bus speeds as a function of distance. These signals, together with the vertical bridge excitation signals (Fig. 6), are used to establish vertical excitations of the coach model's left and right wheel tracks (Sekulic et al., 2021). The magnitude of roll motion gradually increases with storm severity. For W1, roll motion excitation is small and within ± 0.1° (Fig. 9a). For W10, roll motion excitation is large and within ± 1.5° (Fig. 9j).

Wind velocity excitation

Fig. 10 shows a wind velocity signal example in the global coordinate system for a coach speed of 72 km/h for W1–W10. The magnitudes of the horizontal and vertical components gradually increase with storm severity. The along-wind and cross-wind signals were used for relative wind velocity calculations and aerodynamic force/moment calculations (Sekulic et al., 2021). In comparison to the horizontal wind components, the vertical wind component was deemed minor and therefore not considered in aerodynamic load calculations (Sekulic et al., 2021).

Fig. 11 presents the *RMS* values for each wind component. For each coach speed, the *RMS* values for the along-wind and cross-wind components rise with storm intensity. The *RMS* values are low for the vertical wind component (below 2 m/s, Fig. 11c). The maximum *RMS* value for the horizontal wind components is approximately 20 m/s, as shown in Fig. 11a–b.

Simulation results and discussion

The simulation results for 10 storm conditions (W1–W10) are presented in this section. A large quantity of results was obtained, and only the bus model responses in characteristic cases are shown here.

Analysis of lateral path and traffic lane deviation

Vehicle path tracking

Fig. 12 shows the simulation results for path tracking for storm condition W5, as an example. It could be noticed that the vehicle's course deviates from the path more with increasing its speed. Soon after the bus enters the bridge, the highest path deviations occur for speeds of 90 km/h and 108 km/h (approximately 0.5 m; Fig. 12 d-e). Path deviations remain at 0.5 m along the bridge at a bus speed of 108 km/h (Fig. 12e). With increasing bus speed, the *RMS* value of lateral displacement rises (Fig. 12f). Additionally, the maximum deviation increases with increasing bus speed (Fig. 12g). For speeds of 92 km/h and 108 km/h, the maximum deviations are 0.5 m and 0.7 m, respectively (Fig. 12g).

Fig. 13 presents the simulation results for path tracking under ten storm conditions (W1-W10) and for a bus speed of 90 km/h. As the storm gets stronger, the deviation from the path increases. Notably, the deviation is low for W1 (approximately 0.05 m) and high for W7 (approximately 0.7 m) shortly after the bus comes in the bridge section. The vehicle is unstable under strong storm conditions (W8, W9, and W10), and path deviations sharply increase (Fig. 13 h-j).

Fig. 14 shows the *RMS* values and absolute values of maximum vehicle path deviation as a function of coach speed and storm conditions for the cases in which the vehicle can be safely operated (i.e., no risk of bus rollover, and the bus is stable; Table 3). Both parameters increase with the bus speed and storm severity. The highest *RMS* value is close to 0.3 m for a speed of 108 km/h and storm condition W5 (Fig. 14a). The highest value of maximum path deviation is close to 0.8 m for a speed of 90 km/h and storm condition W7 (Fig. 14b).

Traffic lane departure

Lateral displacement from the path increases with coach speed and storm severity (Fig. 14). As a result, it is crucial to ascertain whether the coach leaves the traffic lane. Fig. 15 presents the outermost points of the vehicle, which are considered when analysing leaving the traffic lane. Important bus parameters, such as total length (L_{BUS}), total width (W_{BUS}), and front and rear overhang (f_{oh_bus}, r_{oh_bus}), are also signified in

Table 1
Ten storm conditions (W1–W10).

Storm condition	Waves			Swell			Wind - [1hr - 10m]	
	Dir [°]	Hs [m]	Tp [s]	Dir [°]	Hs [m]	Tp [s]	Dir [°]	ws [m/s]
W1 (<1-year storm)	315.00	0.20	2.07	300.00	0.04	17.00	315.00	6.13
W2 (<1-year storm)	315.00	0.40	2.73	300.00	0.07	17.00	315.00	9.84
W3 (<1-year storm)	315.00	0.60	3.22	300.00	0.11	17.00	315.00	13.08
W4 (<1-year storm)	315.00	0.80	3.61	300.00	0.15	17.00	315.00	15.99
W5 (<1-year storm)	315.00	1.00	3.96	300.00	0.18	17.00	315.00	18.73
W6 (1-year storm)	315.00	1.20	4.26	300.00	0.22	17.00	315.00	21.40
W7 (2-year storm)	315.00	1.40	4.53	300.00	0.25	17.00	315.00	23.60
W8 (10-year storm)	315.00	1.60	4.78	300.00	0.28	17.00	315.00	25.80
W9 (50-year storm)	315.00	1.80	5.02	300.00	0.33	17.00	315.00	28.50
W10 (100-year storm)	315.00	2.00	5.24	300.00	0.34	17.00	315.00	29.60

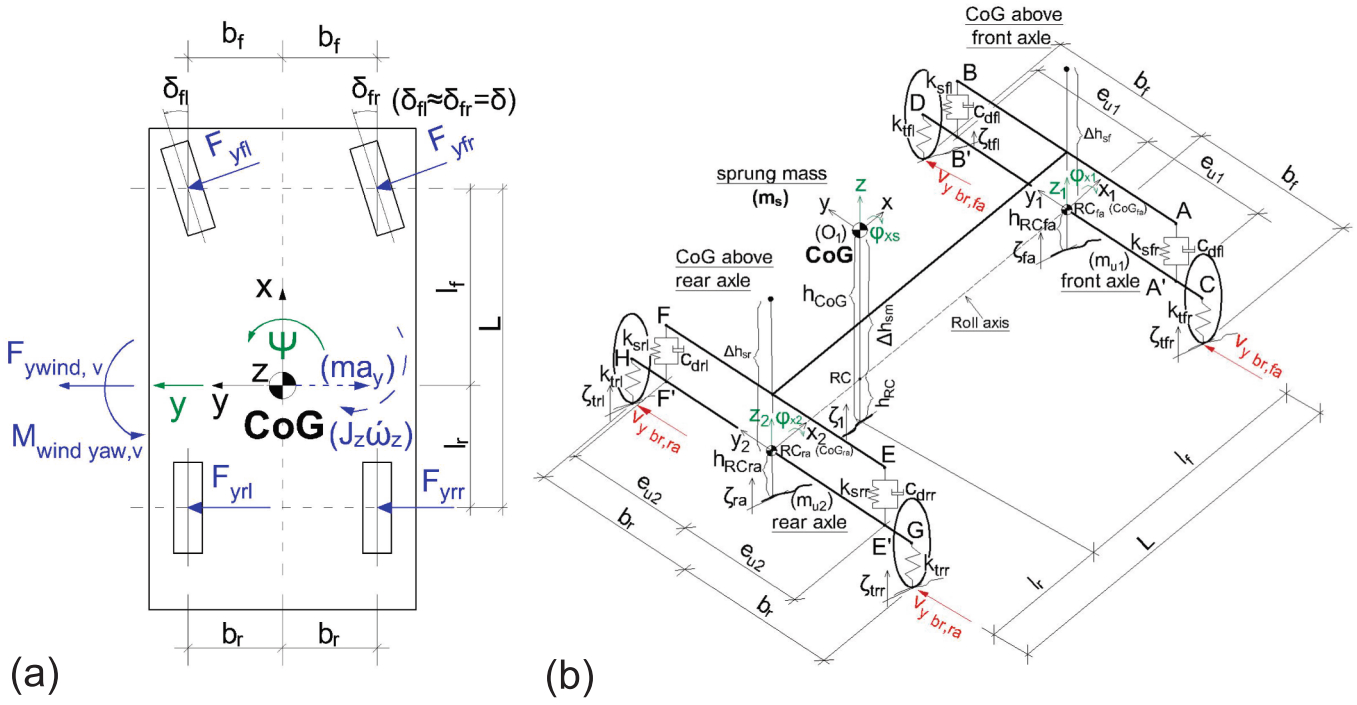

Fig. 2. Eight-DoF bus model: a) In-ground-plane motions, and b) Out-of-ground-plane motions.

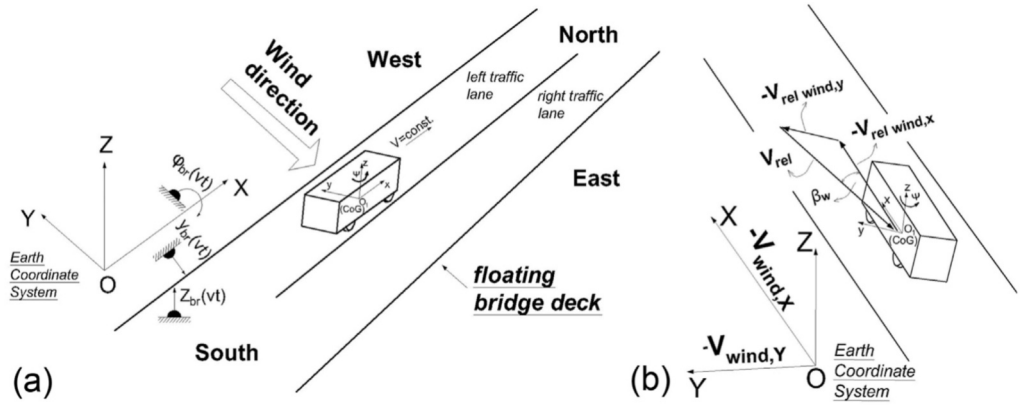

Fig. 3. Coach model excitations from a) floating bridge, and b) wind.

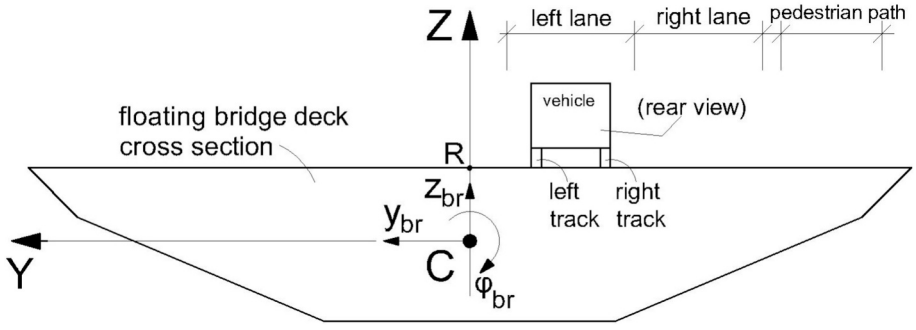

Fig. 4. Bridge deck cross section.

this figure. Table 2 lists the bus parameters.

Fig. 16 shows the path of the outermost vehicle's body points for storm conditions W1-W5. The simulation results show that the coach does not leave the traffic lane under mild storm conditions (W1–W2), regardless of vehicle speed. Fig. 16a–b shows the outermost body positions within the traffic lane for the highest speed of 108 km/h for W1 and W2. The bus stays in the traffic lane for storm condition W3 at a speed of 90 km/h (Fig. 16c). At a speed of 108 km/h under W3, the

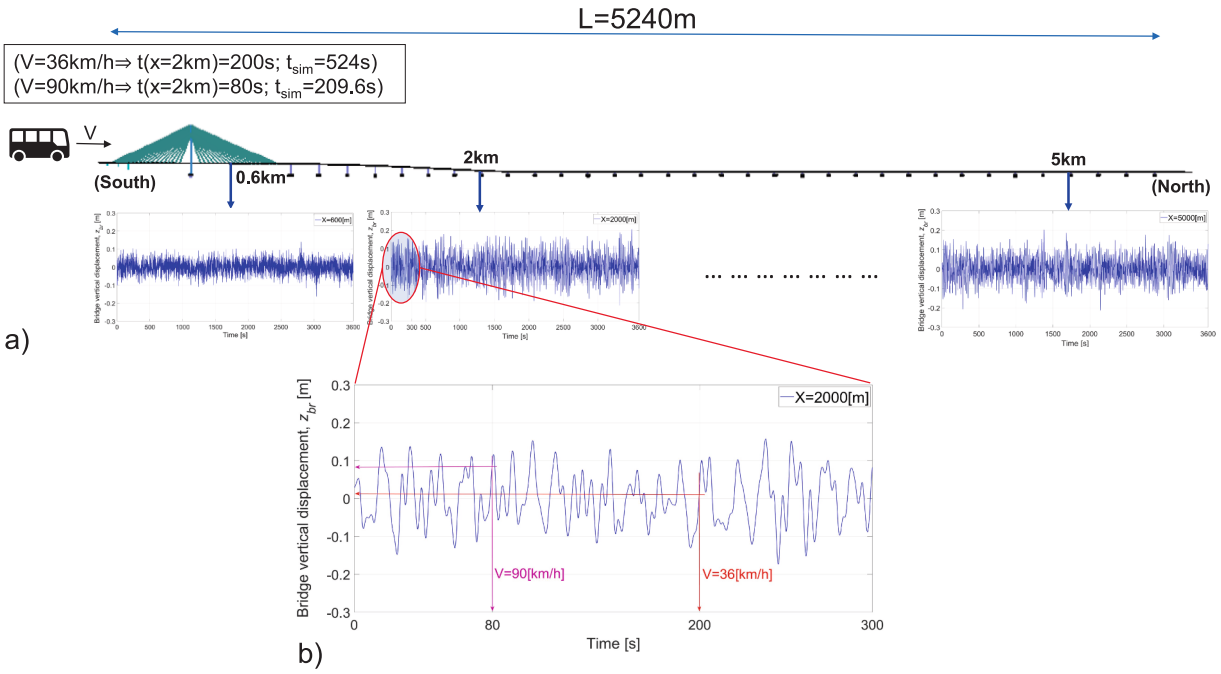

Fig. 5. Vertical bridge displacement a) at distance of 0.6 km, 2 km, 5 km, and b) magnified view for distance of 2 km.

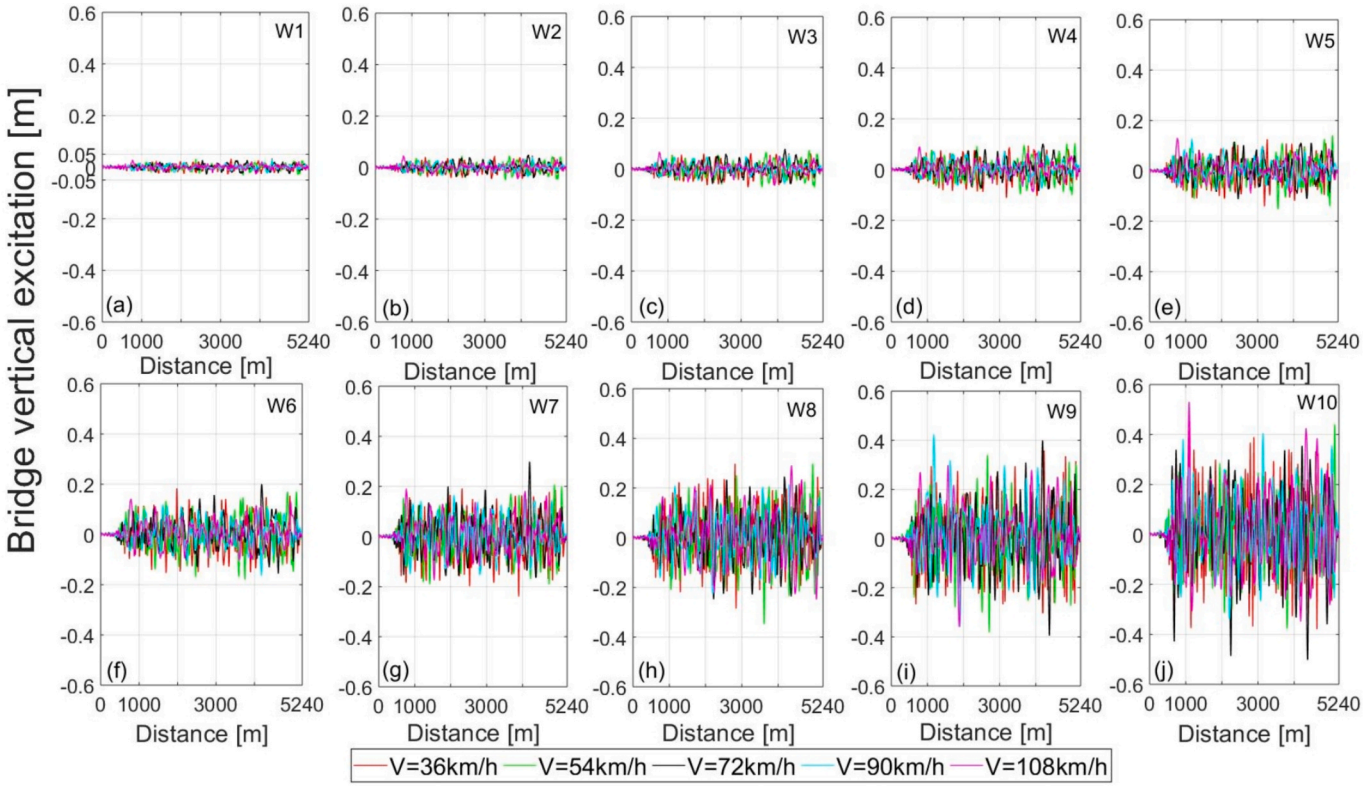

Fig. 6. Vertical bridge excitation for ten storm conditions (W1–W10) as a function of coach speed.

outermost points on the left side of the bus departure the traffic lane slightly when entering the bridge section and at close to 3 km from the beginning of the bridge section (Fig. 16d). At 72 km/h and under W4 and W5 conditions, the vehicle does not leave the lane (Figs. 16e,h); however, at 90 km/h, the bus leaves the lane soon after entering the bridge section (Figs. 16f,i). At a speed of 108 km/h, the bus departures the traffic lane relatively frequently under W4 conditions (Fig. 14g) and often under W5 conditions (Fig. 16j).

Fig. 17 shows the path of the outermost body points of the coach under storm conditions W6-W8. For W6, the bus stays in the traffic lane at speeds of 54 km/h and 72 km/h (Figs. 17a,b), whereas at 90 km/h, it frequently leaves the lane (Fig. 17c). Under W7 and W8 conditions, the bus does not leave the lane at a speed of 54 km/h (Figs. 17d,g) but at 72 km/h, the vehicle slightly leaves the lane along the bridge (Figs. 17e,h).

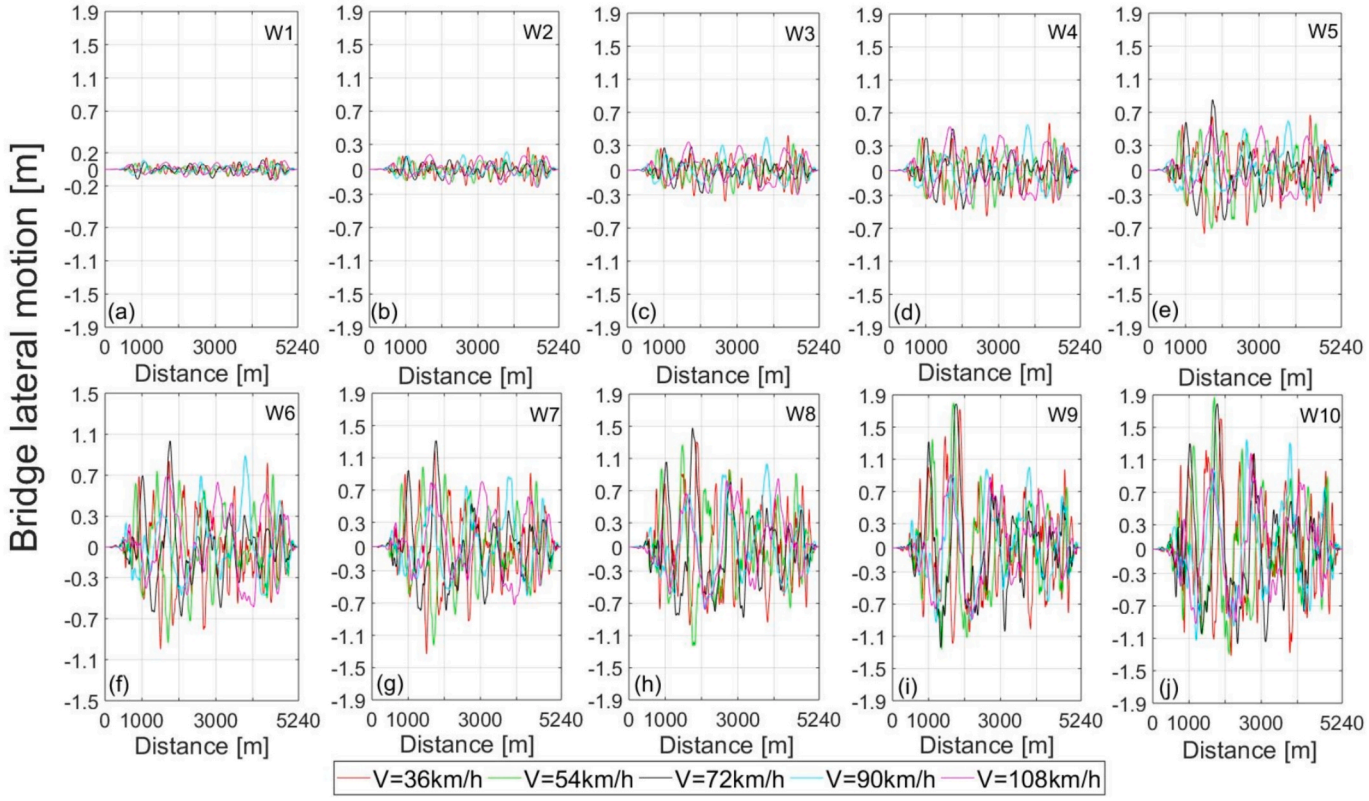

Fig. 7. Lateral bridge motion for ten storm conditions (W1–W10) as a function of coach speed.

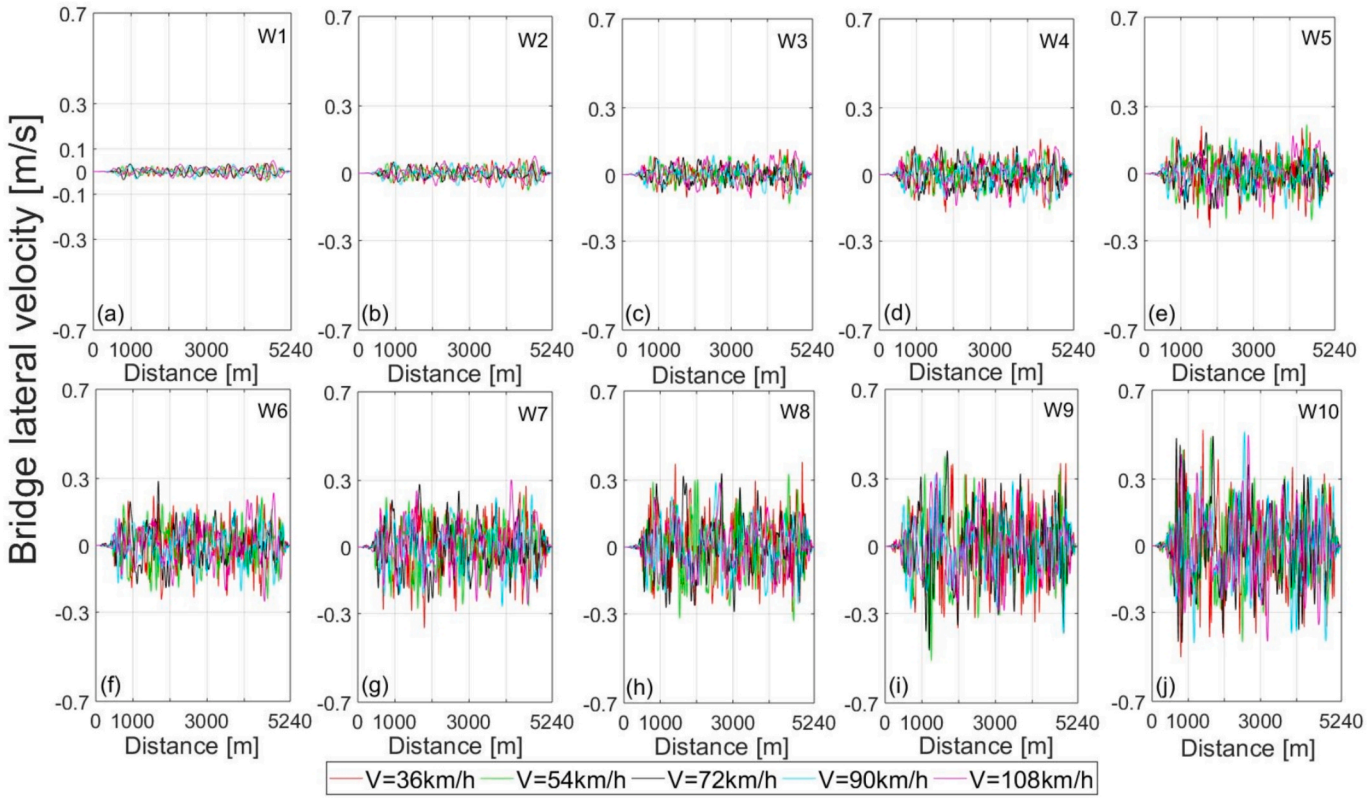

Fig. 8. Lateral bridge velocities for ten storm conditions (W1–W10) as a function of coach speed.

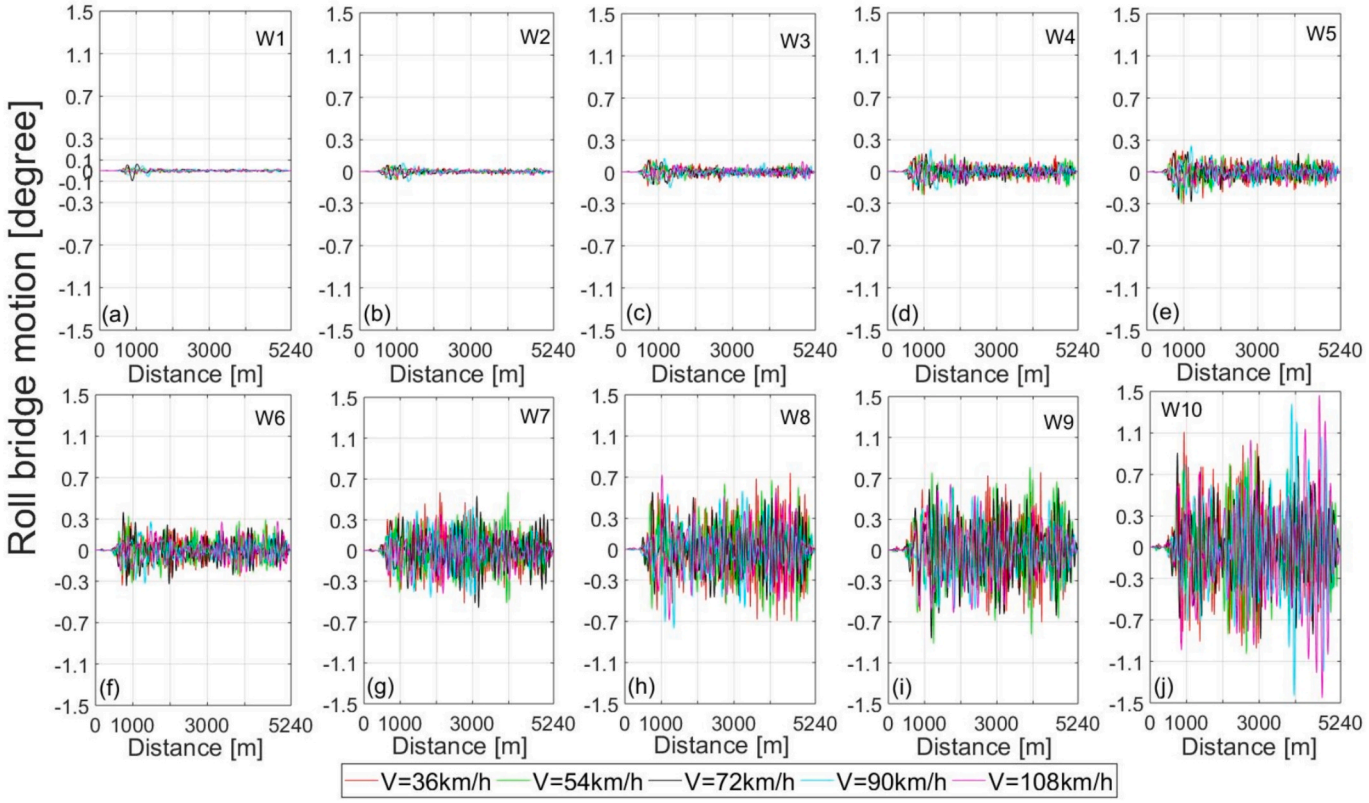

Fig. 9. Bridge roll motion for ten storm conditions (W1–W10) as a function of coach speed.

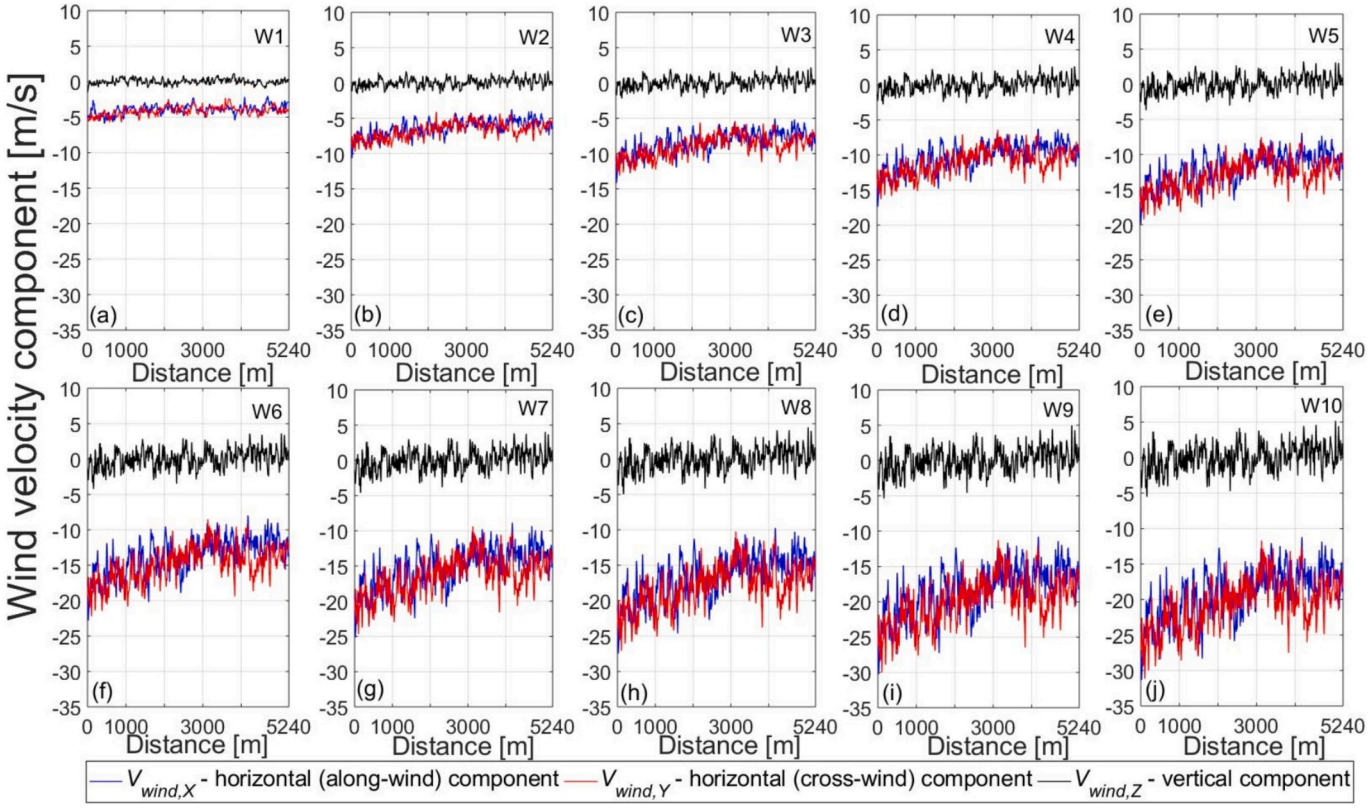

Fig. 10. Wind velocity components for ten storm conditions (W1–W10) at a coach speed of 72 km/h as a function of distance.

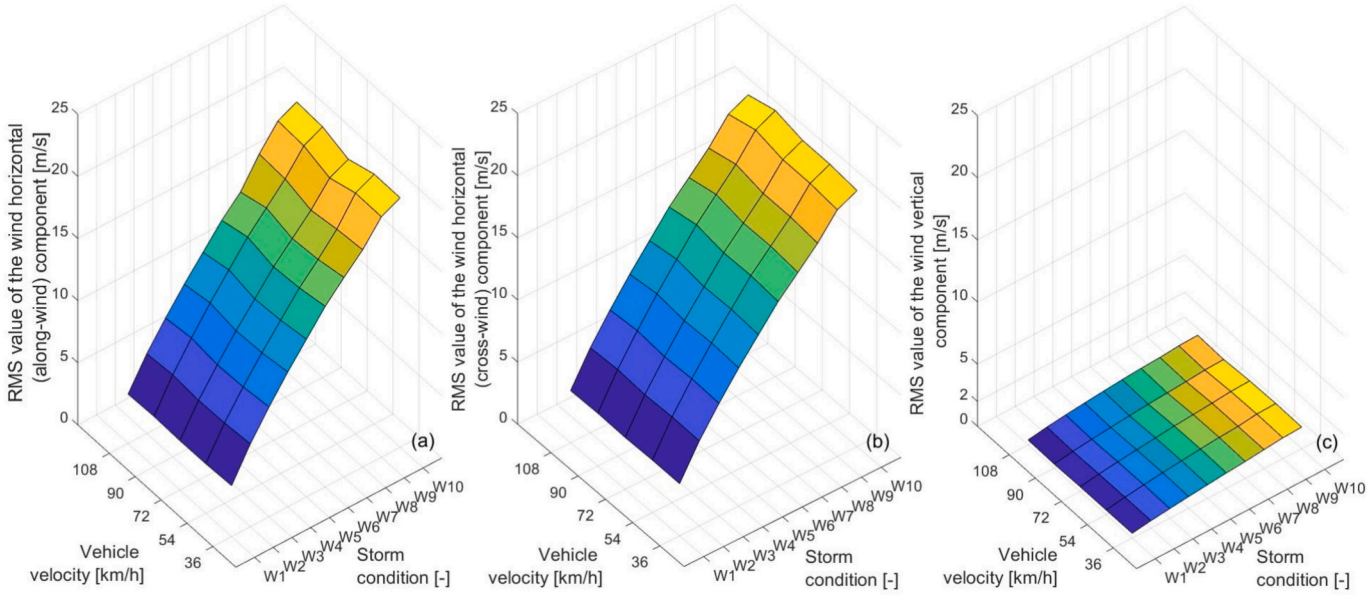

Fig. 11. RMS values for wind components: a) horizontal (along-wind) component, b) horizontal (cross-wind) component, and c) vertical component.

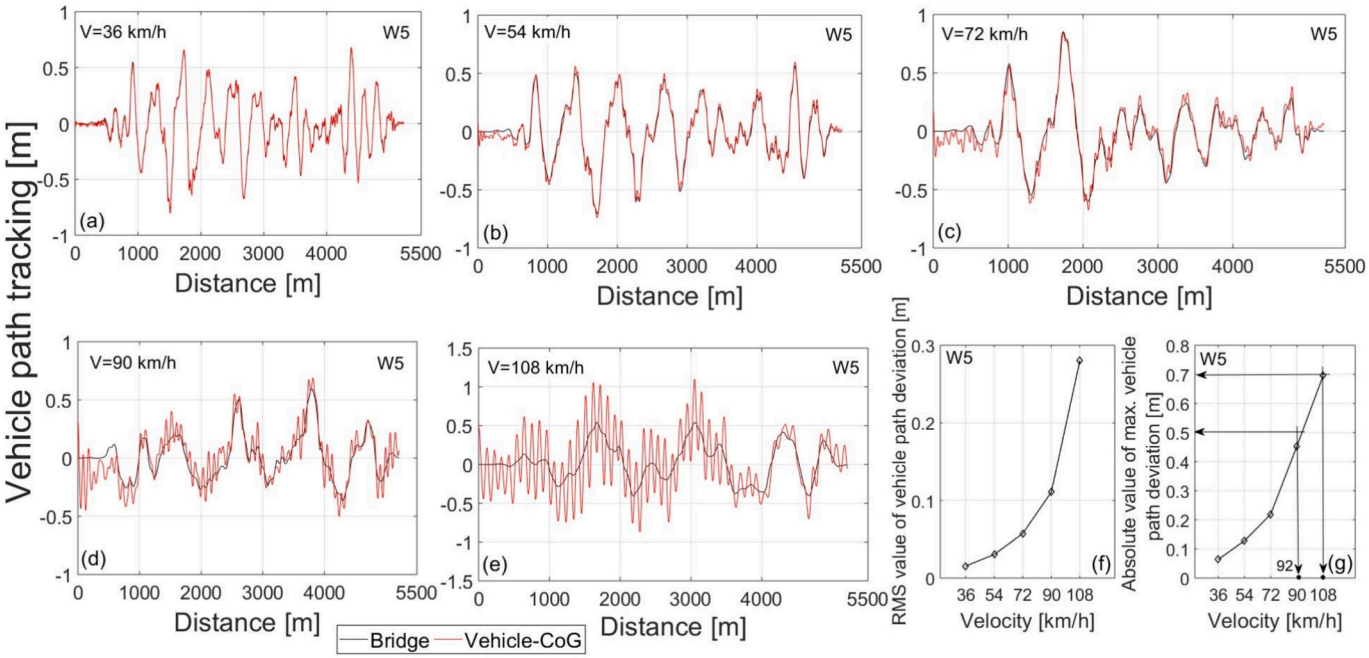

Fig. 12. Path tracking for bus speeds a) of 36 km/h, b) of 54 km/h, c) of 72 km/h, d) of 90 km/h, e) of 108 km/h, f) RMS values, and g) absolute value of max. path deviation for storm condition W5.

Under W7 and at a speed of 90 km/h, the bus severely and frequently leaves the traffic lane (Fig. 17f).

Steering effort of the driver

Fig. 18 presents the handwheel steering angle (HSA) as a function of distance and speed for W1-W8. The HSA intensity increases with increasing vehicle speed for each storm condition. Additionally, the HSA intensity increases with the severity of the storm. For instance, at a speed of 108 km/h, the maximum HSA value is approximately 12 degrees (Fig. 18a) for W1 and approximately 50 degrees for W5 (Fig. 18e).

It could be seen that the HSA signals deviate around a certain mean value in each case (Fig. 18), and the *RMS* and mean values increase with the vehicle speed and storm severity (Fig. 19).

Roll-over risk

Simulation results confirmed that vertical tire forces (VTFs) are positive at every speed and under storm conditions W1-W5. Fig. 20 depicts the VTFs for each coach wheel as a function of time for a speed of 108 km/h and W1-W7 conditions. Notably, the VTFs increase with storm severity. In addition, the winward wheels' VTFs are less values than those of the windward wheels. Both windward wheels (left front and rear wheels) lose contact with the floating bridge deck at a speed of 108 km/h for W6 and W7 (Figs. 20g,i). The loss of contact with both windward wheels leads to the simulation stopping at approximately 40 s

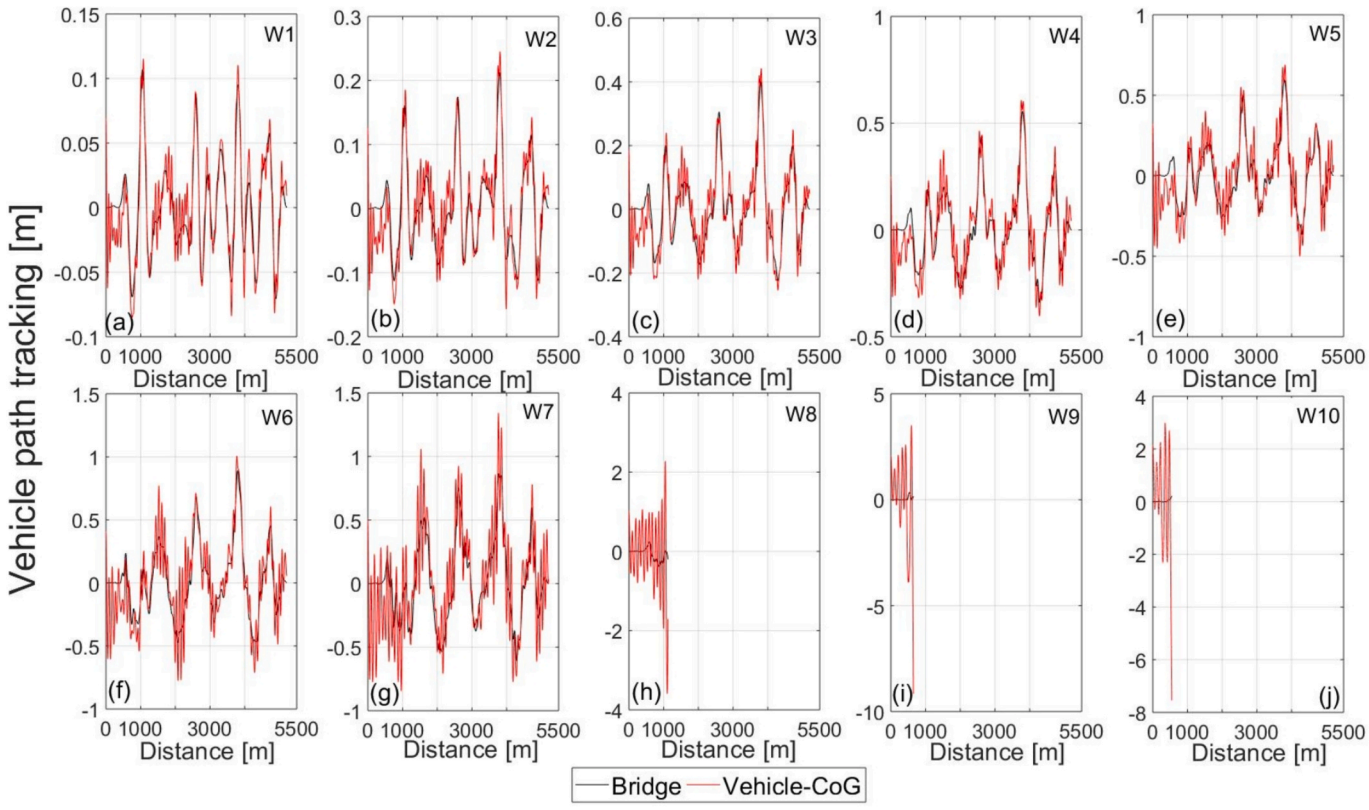

Fig. 13. Path tracking under ten storm conditions (W1–W10) at a bus speed of 90 km/h.

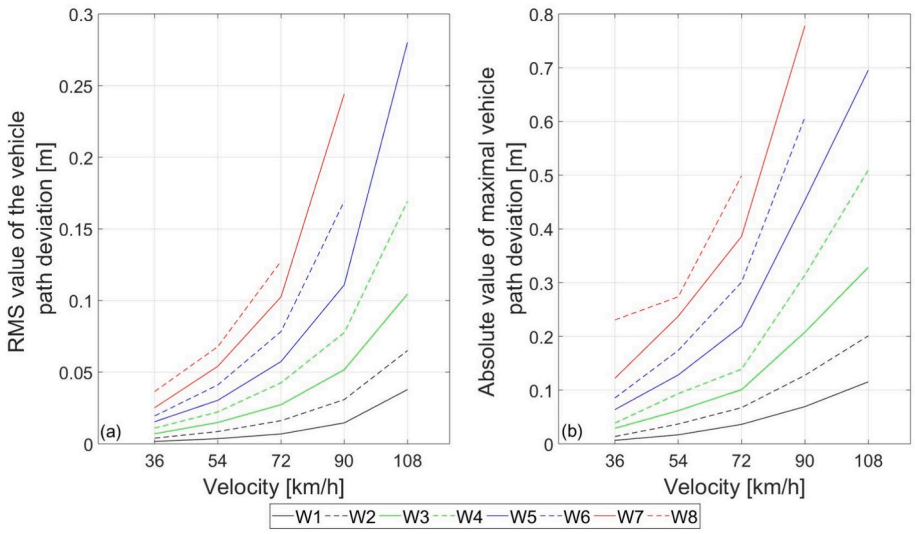

Fig. 14. Vehicle path deviation: a) RMS value, and b) absolute maximum value for different storm conditions as function of vehicle speed.

(Figs. 20g,i). At a speed of 90 km/h, the VTFs are greater than zero (Figs. 20f,h).

Simulation results confirmed that both windward wheels of the bus separate from the bridge deck at 90 km/h and 108 km/h under storm conditions W8, W9 and W10. At speeds of 36 km/h, 54 km/h and 72 km/h and for both W9 and W10, the rear wheel on the vehicle windward side loses contact frequently along the bridge (Figs. 21c,e). At 36 km/h, the rear wheel on the vehicle windward side separates from the deck soon after the vehicle enters the bridge section under W8 conditions. This happens in one short interval of simulation time (less than 0.2 s; Figs. 21a,d). At the same time, a significant load reduction is observed at the windward front wheel (approximately 1 s; Fig. 21d). Therefore, the speed of 36 km/h for W8 is not considered unsafe.

Load transfer ratio (LTR)

Risk of vehicle roll-over is commonly predicted using the LTR parameter (Kamnik et al., 2003) according to Eq. (2). If the *LTR* is larger than 0.9 (i.e., the left or right vehicle tires separate from the ground), the vehicle is considered to overturn (Wang et al. (2016)).

$$LTR = \frac{Z_{tfl} + Z_{trl} - Z_{tfr} - Z_{trr}}{Z_{tfl} + Z_{tfr} + Z_{trl} + Z_{trr}} \tag{2}$$

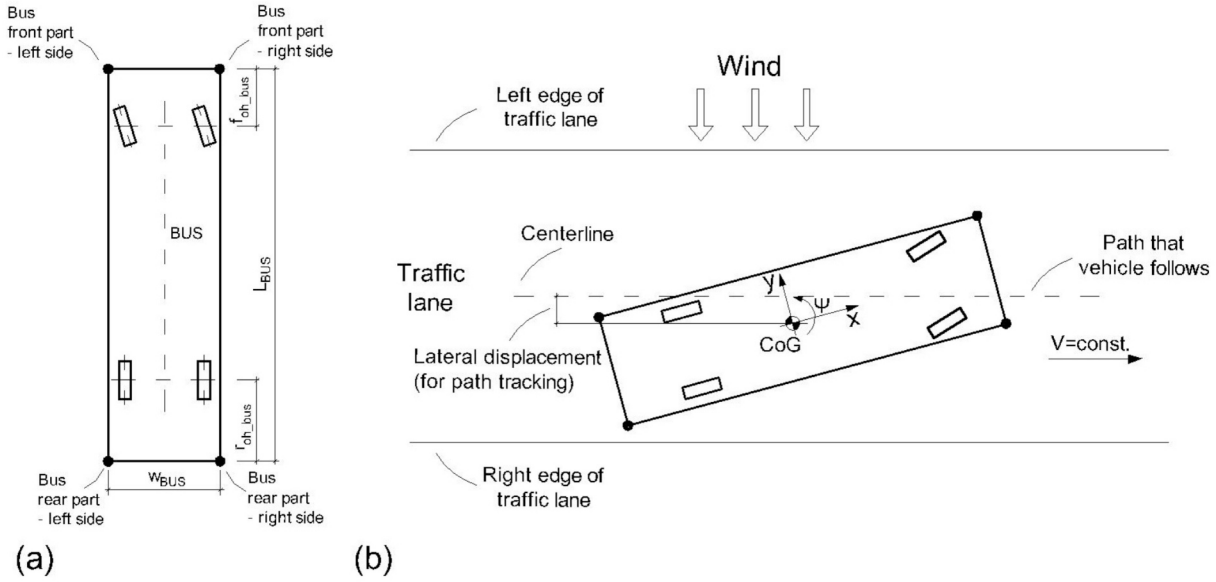

Fig. 15. Outermost body points of the bus a) at the vehicle front and rear sections, and b) the bus position within the traffic lane.

Table 2
Bus parameters.

Bus parameters	Values
Length, L_{BUS} [m]	13.80
Width, W_{BUS} [m]	2.535
Front overhang, f_{oh_bus} [m]	2.619
Rear overhang, r_{oh_bus} [m]	2.806

where Z_{tfl}, Z_{tfr}, Z_{trl}, and Z_{trr} are the vertical tire forces for the front left, front right, rear left, and rear right wheels, respectively.

Fig. 22 presents the maximum absolute *LTR* value for storm conditions W1-W8 as a function of speed. The *LTR* value increases with storm severity. There is no risk of vehicle rollover for W1-W5. For storm conditions W6, W7 and W8, *LTR* values are larger than 0.9 for speeds above 100 km/h, 96 km/h and 82 km/h, respectively, indicating vehicle rollover risk.

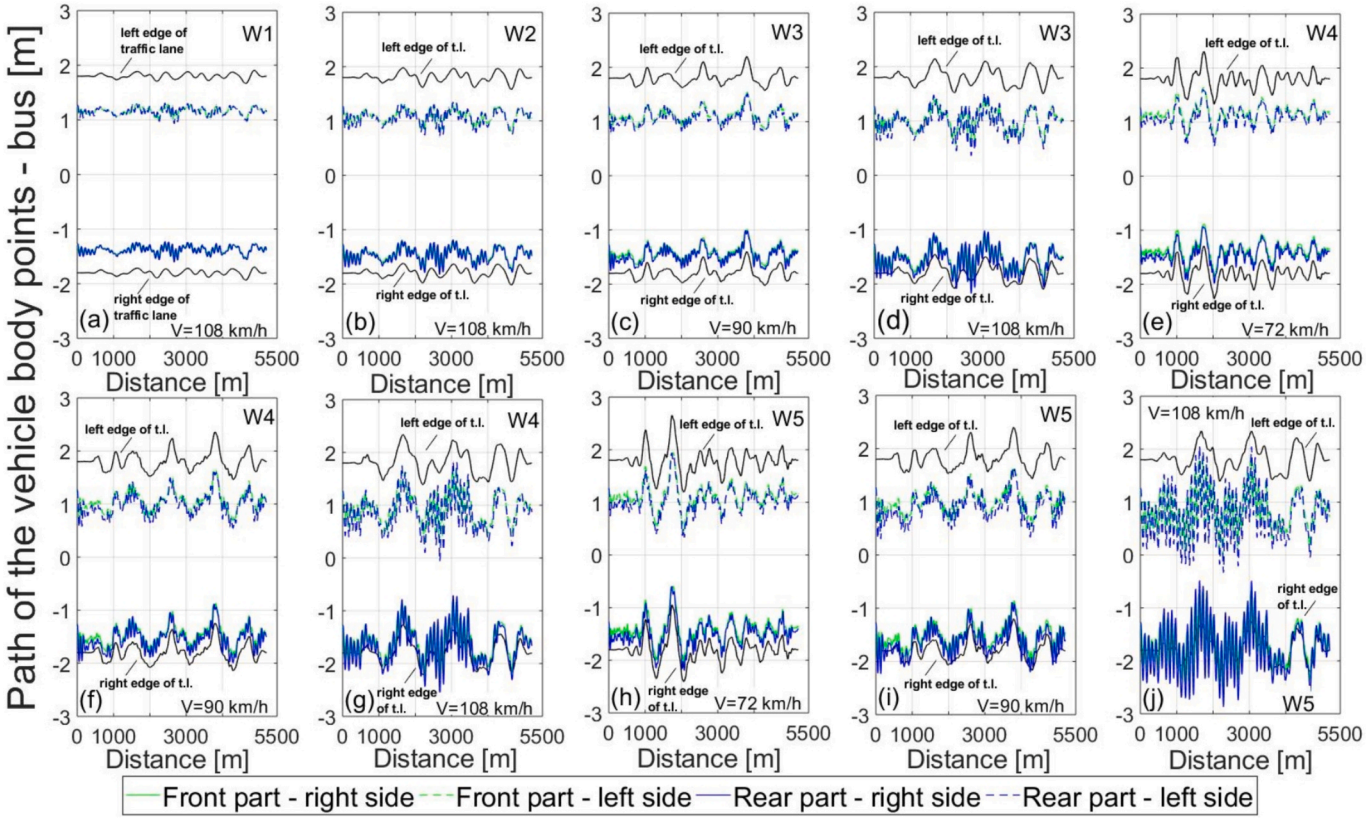

Fig. 16. Path of the outermost bus body points at a) 108 km/h for W1, b) 108 km/h for W2, c) 90 km/h for W3, d) 108 km/h for W3, e) 72 km/h for W4, f) 90 km/h for W4, g) 108 km/h for W4, h) 72 km/h for W5, i) 90 km/h for W5, and j) 108 km/h for W5.

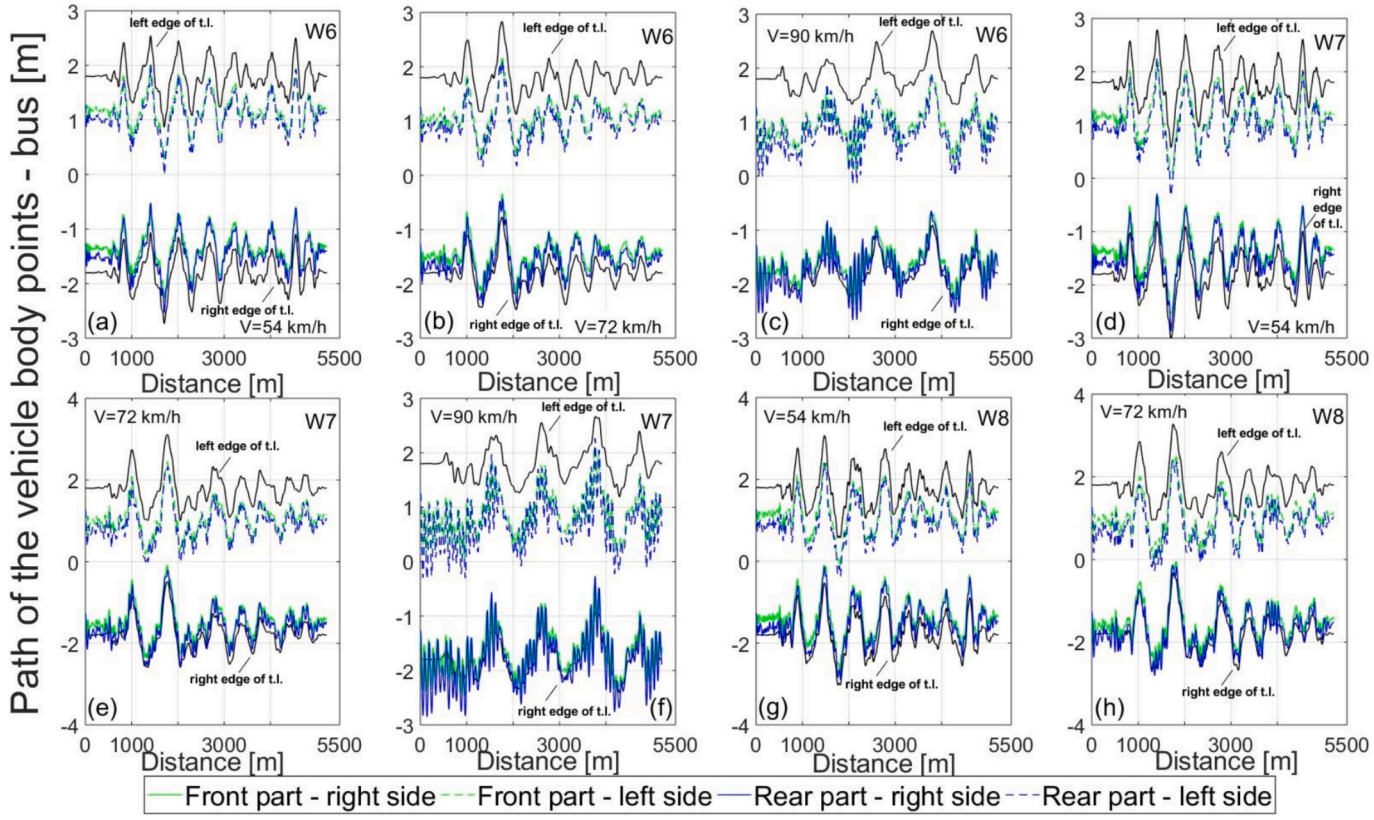

Fig. 17. Path of the outermost body points of the bus at a) 54 km/h for W6, b) 72 km/h for W6, c) 90 km/h for W6, d) 54 km/h for W7, e) 72 km/h for W7, f) 90 km/h for W7, g) 54 km/h for W8, and h) 72 km/h for W8.

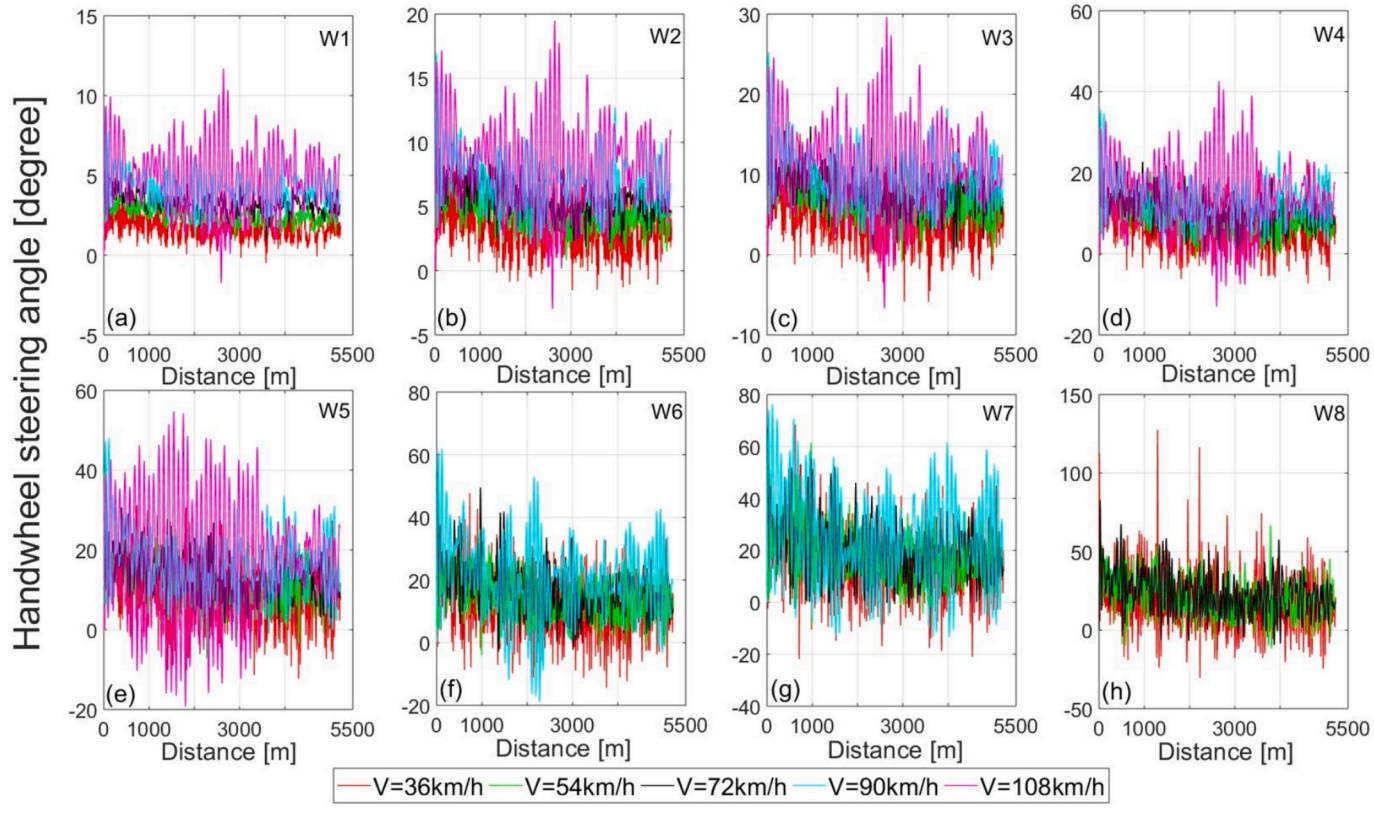

Fig. 18. HSA as a function of distance, storm conditions (W1–W8) and vehicle speeds.

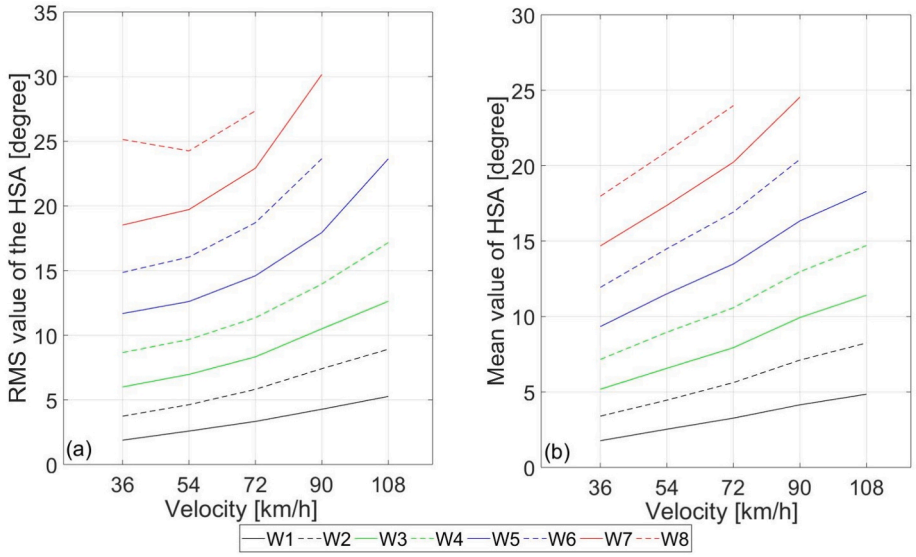

Fig. 19. HSA: a) RMS values, and b) mean values for different storm conditions as a function of speed.

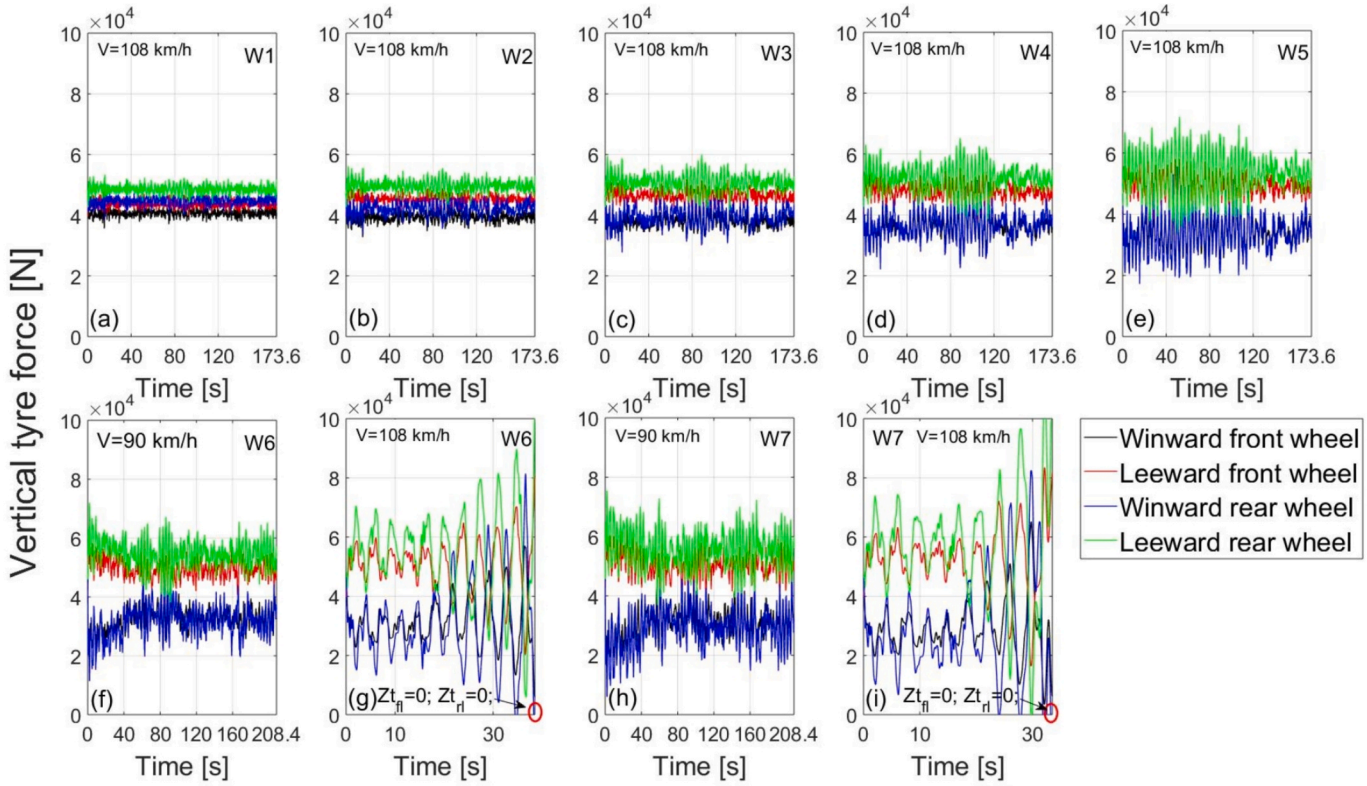

Fig. 20. Vertical tire forces for different storm conditions (W1–W7) as a function of time and bus speed.

Losing lateral grip analysis

Lateral sideslip limit (LSL)

The risk of losing lateral grip can be analysed based on the *LSL* parameter (Chen and Chen, 2011; Chen and Chen, 2010), as shown in Eq. (3).

$$LSL = \min\left[F_{y,fa}^{max} + F_{y,ra}^{max} - \left(F_{y,fa} + F_{y,ra}\right)\right] = \min\left[\mu\cdot\left(Z_{t,fa} + Z_{t,ra}\right) - \left(F_{y,fa} + F_{y,ra}\right)\right] \geq 0 \quad (3)$$

where $F_{y,fa}^{max}$ and $F_{y,ra}^{max}$ are the maximum values of the lateral friction forces that could be realized on front and rear axles, respectively, for a given road surface; $Z_{t,fa}$ and $Z_{t,ra}$ are the vertical forces on the front and rear bus axles, respectively; $F_{y,fa}$ and $F_{y,ra}$ are the actual lateral tire forces for the front and rear bus axles, respectively; and μ is the road friction coefficient (value of 0.7 for dry-wet asphalt pavement surface (Shin and Lee, 2015)). If the *LSL* value is less than zero, the vehicle starts to experience sideslip.

Fig. 23 shows the minimum *LSL* value for storm conditions W1-W8 as a function of speed. The *LSL* value decreases with the vehicle speed and storm severity. The *LSL* is greater than zero for W1-W5, which means that the *LSL* limit is not reached for the considered road surface. For W6,

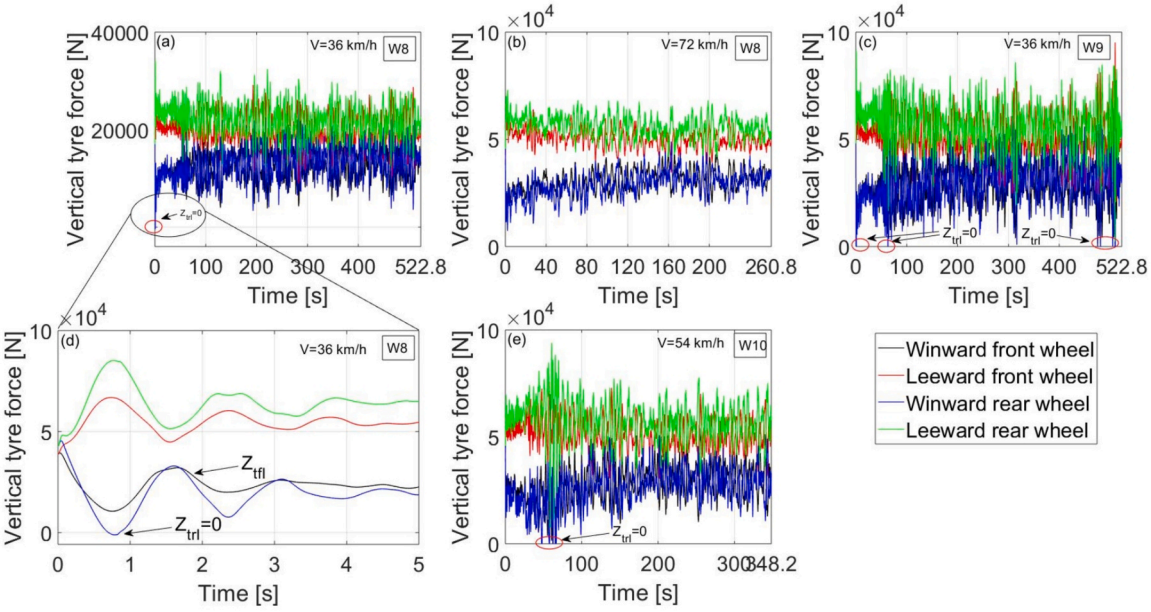

Fig. 21. Vertical tire forces for storm conditions (W8–W10) as a function of time and bus speed.

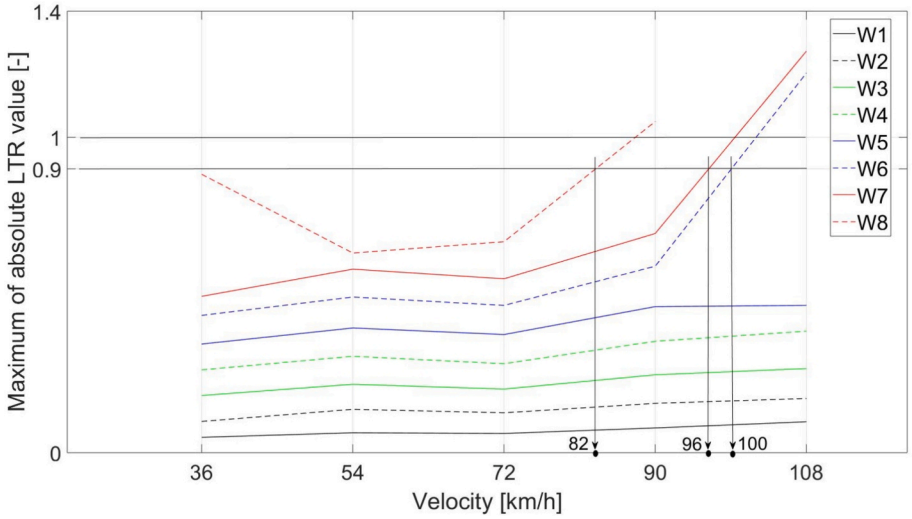

Fig. 22. Maximum absolute LTR value for storm conditions (W1–W8) as a function of speed.

W7 and W8, the *LSL* is greater than or equal to zero for speeds of 108 km/h and 87 km/h, respectively; this indicates that vehicle rollover occurs before vehicle sliding. These results are logical since the road friction coefficient is relatively high (value of 0.7).

Simulation results summary

Table 3 shows a summary of the simulation results for the bus response under storm cases W1–W10. Safe speeds for a coach travelling over the studied bridge under hazardous driving conditions can be determined from this table. The meaning of the colours is explained below Table 3.

The results show that the bus is not stable when moving at 108 km/h for W6–W10 and at 90 km/h for W8–W10. The windward wheel frequently separates from the deck at 36 km/h, 54 km/h and 72 km/h under W9 and W10 conditions. The windward wheel loses contact at 36 km/h for W8 at only one instance of time for a very short period. At 108 km/h for W3–W5, the vehicle leaves the traffic lane when entering the bridge section. At 72 km/h for W6 and W7 conditions, the vehicle departures the traffic lane when entering the bridge section. The vehicle severely leaves the traffic lane at 108 km/h for W4, W5 and W6 conditions, at 90 km/h for W6 and W7 conditions, and at a speed of 72 km/h for W8 conditions.

The interpretation of the colours in Table 3 is as follows: vehicle runs safely (empty green box); one vehicle wheel looses contact with the bridge deck only once for short period of time (green box with one tick); vehicle front/rear right side insignificantly leaves the traffic lane when entering the bridge for short period of time (green box with two ticks); vehicle is instable or frequently leaves the traffic lane (empty red box); vehicle front/rear right side significantly and frequently leaves the traffic lane along the bridge (red box with one cross sign); vehicle wheels losses contact with the bridge deck frequently (red box with two cross signs); vehicle is instable (red box with three cross signs).

Conclusions

In this work, safe speeds are defined for a coach traveling on the planned Bjørnafjorden floating bridge under ten different storm

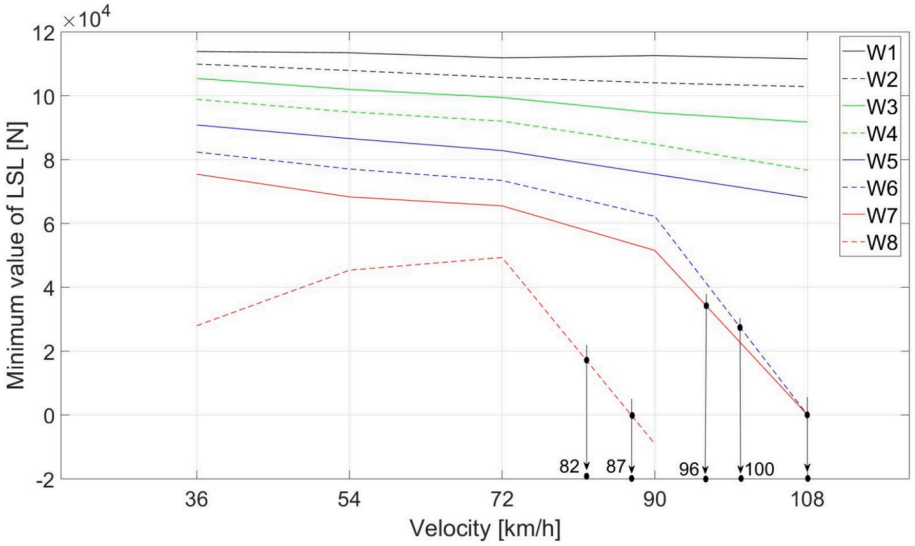

Fig. 23. Minimum value of LSL for storm conditions (W1–W8) as a function of speed.

Table 3
Summary of the simulation results.

Storm condition	Waves			Swell			Wind - [1hr - 10m]	
	Dir [°]	Hs [m]	Tp [s]	Dir [°]	Hs [m]	Tp [s]	Dir [°]	ws [m/s]
W1 (<1-year storm)	315.00	0.20	2.07	300.00	0.04	17.00	315.00	6.13
W2 (<1-year storm)	315.00	0.40	2.73	300.00	0.07	17.00	315.00	9.84
W3 (<1-year storm)	315.00	0.60	3.22	300.00	0.11	17.00	315.00	13.08
W4 (<1-year storm)	315.00	0.80	3.61	300.00	0.15	17.00	315.00	15.99
W5 (<1-year storm)	315.00	1.00	3.96	300.00	0.18	17.00	315.00	18.73
W6 (1-year storm)	315.00	1.20	4.26	300.00	0.22	17.00	315.00	21.40
W7 (2-year storm)	315.00	1.40	4.53	300.00	0.25	17.00	315.00	23.60
W8 (10-year storm)	315.00	1.60	4.78	300.00	0.28	17.00	315.00	25.80
W9 (50-year storm)	315.00	1.80	5.02	300.00	0.33	17.00	315.00	28.50
W10 (100-year storm)	315.00	2.00	5.24	300.00	0.34	17.00	315.00	29.60

conditions (W1–W10). The storm conditions differ in terms of the wave, swell and wind characteristics.

The following are the main results drawn from this study:

- With increasing bus speed and storm intensity, vehicle departure from the path increases. Consequently, the load on the bus driver required to keep the vehicle within a traffic lane increases as the weather conditions become increasingly severe.
- At 90 km/h for W4 and W5, the vehicle leaves the traffic lane only when entering the bridge section. The bus can enter the bridge section safely at a speed of 90 km/h, and the bus speed can be increased to 108 km/h after 0.5 km of travel.
- At 72 km/h for W6 and W7, the vehicle departures the traffic lane when entering the bridge section only. The bus can safely enter the bridge section at a speed of 54 km/h, and the bus speed can be increased to 72 km/h after 0.5 km of travel.
- At 108 km/h for W4, W5 and W6, the vehicle leaves the traffic lane severely and frequently; the same issue occurs at a speed of 90 km/h for W6 and W7 and at a speed of 72 km/h for W8. Therefore, these speeds are not safe.
- At 108 km/h for W6–W10 and at a speed of 90 km/h for W8, W9, and W10, the bus is not stable. Therefore, these speeds are not safe.
- At 36 km/h for W8, the windward wheel of the bus separates from the deck at only one instance of time for a very short period. Thus, this speed is not considered unsafe.
- At speeds of 36 km/h, 54 km/h and 72 km/h for W9 and W10, the windward wheels of the bus frequently separate from the bridge deck. Therefore, these speeds are not safe.

Considering the results and findings from this work, useful recommendations and measures could be determined to help bridge management in maintaining safe coach speeds over floating bridge under hazardous driving conditions.

CRediT authorship contribution statement

Dragan Sekulic: Conceptualization, Visualization, Writing – review & editing, Data curation, Methodology, Writing – original draft. **Alexey Vdovin:** Supervision, Conceptualization. **Bengt Jacobson:** Conceptualization, Supervision, Writing – review & editing, Methodology, Validation. **Simone Sebben:** Conceptualization, Supervision. **Stian Moe Johannesen:** Resources, Investigation.

Declaration of competing interest

The authors declare that they have no known competing financial interests or personal relationships that could have appeared to influence the work reported in this paper.

Acknowledgments

The Norwegian Public Road Administration (NPRA) provided support for this research. Swedish National Infrastructure for Computing (SNIC) provided resources for aerodynamic simulations at the National Supercomputer Centre (NSC). This research was partially funded by the Swedish Research Council through grant agreement no. 2018-05973. These supports are gratefully acknowledged.

Appendix

.

Table A4
Coach parameters.

Geometric parameters of the bus	
Wheelbase L [m]	8.375
Front overhang f_{oh} [m]	2.619
Rear overhang r_{oh} [m]	2.806
Distance from the front axle to the centre of gravity (CoG) of an empty bus l_f [m]	4.4103
Distance from the rear axle to the centre of gravity (CoG) of empty bus l_r [m]	3.9647
Distance from the front right/left wheel to the front axle CoG b_f [m]	1.00
Distance from the rear right/left wheel to the rear axle CoG b_r [m]	1.00
Distance from the CoG of the whole vehicle to the ground $h_{CoG,stat.}$ [m]	1.1725
Height of the front axle roll-centre $h_{RCfa,stat.}$ [m]	0.508
Height of the rear axle roll-center $h_{RCra,stat.}$ [m]	0.508
Distance from the CoG to the roll-centre for the front axle $h_{RCfa,stat.}$ [m]	0.6645
Distance from the CoG to the roll-centre for the rear axle $h_{RCra,stat.}$ [m]	0.6645
Distance from suspension elements on the front axle to the front axle CoG e_{u1} [m]	0.70
Distance from suspension elements on the rear axle to the rear axle CoG e_{u2} [m]	0.80
Mass parameters of the bus	
Sprung mass of the empty bus m_s [kg]	16,099
Front axle – mass m_{u1} [kg]	746
Rear axle – mass m_{u2} [kg]	1355
Empty bus – mass m [kg]	18,200
Sprung mass – moment of inertia about its x-axis J_{sx} [kgm^2]	33,400
Sprung mass – moment of inertia about its y-axis J_{sy} [kgm^2]	150,000
Bus – moment of inertia about z-axis J_z [kgm^2]	290,000
Front axle – moment of inertia relative to the x_1-axis J_{ux1} [kgm^2]	315
Rear axle – moment of inertia relative to the x_2-axis J_{ux2} [kgm^2]	657
Oscillatory parameters of the bus	
Stiffness for one air spring on the front axle k_{sf} [N/m]	175,000
Stiffness for all air springs on the front axle k_{sfeq} [N/m]	350,000
Damping for one shock-absorber on the front axle c_{df} [Ns/m]	20,000
Damping for all shock-absorbers on the left side of the front axle c_{dfl} [Ns/m]	40,000
Damping for all shock-absorbers on the right side of the front axle c_{dfr} [Ns/m]	40,000
Damping for all shock-absorbers on the front axle c_{dfeq} [Ns/m]	80,000
Stiffness for one air spring on the rear axle k_{sr} [N/m]	200,000
Stiffness for all air springs on the left side of the rear axle k_{srl} [N/m]	400,000
Stiffness for all air springs on the right side of the rear axle k_{srr} [N/m]	400,000
Stiffness for all air springs on the rear axle k_{sreq} [N/m]	800,000
Damping for one shock-absorber on the rear axle c_{dr} [Ns/m]	22,500
Damping for all shock-absorbers on the left side of the rear axle c_{drl} [Ns/m]	45,000
Damping for one shock-absorber on the right side of the rear axle c_{drr} [Ns/m]	45,000
Damping for all shock-absorbers on the rear axle c_{dreq} [Ns/m]	90,000
Radial stiffness for one tyre on the left/right side of the front axle k_{tfl}/k_{tfr} [N/m]	1,000,000
Radial stiffness for all tyres on the front axle k_{tfeq} [N/m]	2,000,000
Radial stiffness for one tyre on the left/right side of rear axle k_{trl}/k_{trr} [N/m]	2,000,000
Radial stiffness for all tyres on the rear axle k_{treq} [N/m]	4,000,000
Torsional stiffness for anti-roll bar on front axle K_{arbf} [Nm/rad]	120,000
Torsional stiffness for anti-roll bar on rear axle K_{arbr} [Nm/rad]	120,000
Front axle – roll-stiffness $K_{\varphi f}$ [Nm/rad]	171,500
Front axle – roll-damping $C_{\varphi f}$ [Nms/rad]	39,200
Rear axle – roll-stiffness $K_{\varphi r}$ [Nm/rad]	512,000
Rear axle – roll-damping $C_{\varphi r}$ [Nms/rad]	57,600

Data availability

Data will be made available on request.

References

Bhat et al. 2020. *Driver Influence on Vehicle Track-Ability on Floating Bridges*. TME180 Automotive Engineering Project, Chalmers University of Technology, Gothenburg, Sweden. (https://odr.chalmers.se/handle/20.500.12380/300748,).

Branlard, E., 2010. Wind Energy: Generation of Time Series from a Spectrum. Technical University of Denmark, Denmark.

Chen, F., Chen, S., 2010. Simulation-based assessment of vehicle safety behavior under hazardous driving conditions. J. Transp. Eng. 19 (1), 304–315.

Chen, F., Chen, S., 2011. Reliability-based assessment of vehicle safety in adverse driving conditions. Transp. Res. Part C Emerging Technol. 136 (4), 156–168.
Chen, S.R., Cai, C.S., 2004. Accident assessment of vehicles on long-span bridges in windy environments. J. Wind Eng. Ind. Aerodyn. 92 (12), 991–1024.
Gustafsson, A. et al. 2019. *Driver Influence on Vehicle Track-Ability on Floating Bridges*. Bachelor's thesis in Mechanical Engineering, Department of Mechanics and Maritime Sciences, Chalmers University of Technology, Gothenburg, Sweden. (https://odr.chalmers.se/handle/20.500.12380/256914,).
Han, W et al., *Research status and prospect of wind-vehicle-bridge coupling vibration system*, Journal of Traffic and Transportation Engineering (English Edition), https://doi.org/10.1016/j.jtte.2021.05.002.
Hou, G., Chen, S., Chen, F., 2019. Framework of simulation-based vehicle safety performance assessment of highway system under hazardous driving conditions. Transp. Res. Part C Emerging Technol. 105, 23–36.
Iso 8608, ISO 8608, 1995. Mechanical vibration-road surface profiles-reporting of measured data. International Standards Organization, Switzerland.
Kamnik, R., Boettiger, F., Hunt, K., 2003. Roll dynamics and lateral load transfer estimation in articulated heavy freight vehicles. Automobile Engineering. Proc. Inst. Mech. Eng., Part D: J. Autom. Eng. 217 (11), 985–997.
Sekulic, D. 2018. *Effect of floating bridge vertical motion on vehicle ride comfort and road grip*. (https://www.vegvesen.no/_attachment/2487039/binary/1294853?fast_title=Effect+of+floating+bridge+vertical+motion+on+vehicle+ride+comfort+and+road+grip.pdf).
Sekulic, D., Jacobson, B., Moe, S.J., Svangstu, E., 2020. Effect of floating bridge motion on vehicle ride comfort and road grip. In: The IAVSD International Symposium on Dynamics of Vehicles on Roads and Tracks. Springer, Cham, pp. 1416–1424.
Sekulic, D., Vdovin, A., Jacobson, B., Sebben, S., Johannesen, M.S., 2021. Effects of wind loads and floating bridge motion on intercity bus lateral stability. J. Wind Eng. Ind. Aerodyn. 212 (104589), 1–18.
Shin, J., Lee, I., 2015. Reliability analysis and reliability-based design optimization of roadway horizontal curves using a first-order reliability method. Eng. Optim. 47 (5), 622–641.
Vegvesen, 2017. SBJ-31-C3-MUL-22-RE-100 - Bjørnafjorden, straight floating bridge phase 3, Analysis and design (Base Case).
Vegvesen,2021.https://www.vegvesen.no/globalassets/vegprosjekter/utbygging/ferjefrie39/vedlegg/faktaark/lonnsomhet-for-godstransport.pdf.
Wang, B., Xu, Y., Li, Y., 2016. Nonlinear safety analysis of a running road vehicle under a sudden crosswind. J. Transp. Eng. 142 (2), 04015043.
Wang, T., Han, W., Yang, F., Kong, W., 2014. Wind-vehicle-bridge coupled vibration analysis based on random traffic flow simulation. J. Traffic Transp. Eng. (english Edition) 1 (4), 293–308.